2008 IEEE International Conference on
Robotics and Automation
Pasadena, CA, USA, May 19-23, 2008

Serial Algorithm for High-speed Autofocusing of Cells using Depth From Diffraction (DFDi) Method

Soshiro Makise, Hiromasa Oku, and Masatoshi Ishikawa

Abstract— **In this paper, a new serial algorithm for high-speed autofocusing of cells is proposed. The proposed algorithm extracts depth information of target cells from their diffraction patterns. High-speed focusing of yeast cells with 20 ms response time was demonstrated. Continuous autofocusing of yeast cells with a scanning microscope was also demonstrated. The successful continuous autofocusing suggests that image-based high-throughput measurement of cells could be realized using the proposed algorithm.**

I. INTRODUCTION

With the rapid development being seen in life sciences and biotechnology, automated observation of cells and tissues using microscopes is becoming increasingly important. A critical step in such automated observation is autofocusing. Since the depth of focus of microscopes is usually very shallow, typically on the order of several micrometers, small shifts in the depth direction cause the image of the specimen to easily become out of focus. Thus, autofocusing is essential to keep the object in focus for precise observation. Furthermore, major applications of such automated measurement, such as image cytometry, require high throughput because the number of target specimens tends to be enormous. Therefore, high-speed operation is also important.

Many microscope focusing methods based on the spatial frequency of the acquired image have been proposed [1], [2], [3]. The best focal position providing the highest amount of detail can be estimated from a so-called focus curve formed by sampling the image to obtain a focus score and plotting it against focal position in the depth direction. The best focal position is then found by searching for the peak in the focus curve. However, this sampling takes a considerable amount of time because many images at many focal positions must be individually acquired and processed. Assuming that acquisition and processing of each image takes 40 ms [3] and that 20 samples of the focus score are necessary to estimate the focus curve, the entire autofocus process takes at least 0.8 s.

To solve this problem, Oku et al. proposed the "depth from diffraction" (DFDi) method that estimates the depth of a target cell based on its diffraction pattern [4]. The performance of the proposed method was demonstrated by applying it to three-dimensional tracking of a swimming paramecium. Because this method uses only one defocused image for the estimation, it is capable of high-speed focusing.

S. Makise, H. Oku, and M. Ishikawa are with the Department of Information Physics and Computing, Graduate School of Information Science and Technology, University of Tokyo, Hongo 7-3-1, Bunkyo-ku, Tokyo, Japan {Soshiro_Makise, Hiromasa_Oku, Masatoshi_Ishikawa}@ipc.i.u-tokyo.ac.jp

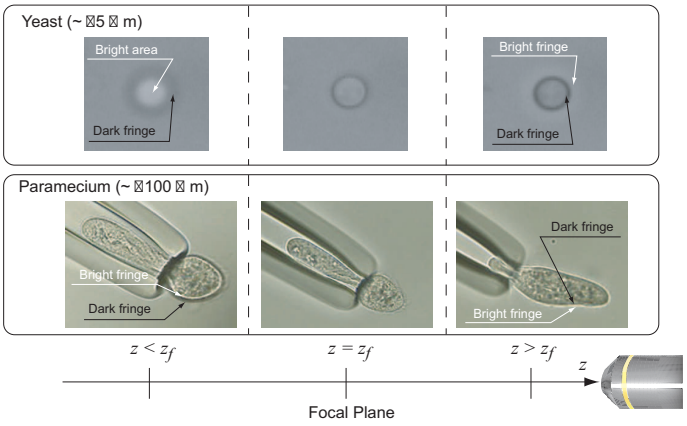

Fig. 1. Diffraction images of yeast and paramecium cells at three focal positions. The yeast cell has a spherical body about 5 μm in diameter. Paramecium is a motile cell with an ellipsoidal body whose longitudinal length is from 100 to 200 μm. The paramecium cell was held in a micro-capillary to keep it in the field of view. In the case of the yeast cell, an intensity variance was observed in the interior of the cell. For $z < z_f$, no clear inner fringe was observed in the yeast cell, but a bright inner area was observed.

The image processing algorithm described in that study, however, could handle only a single cell. To remove this restriction, Makise et al. proposed an autofocusing algorithm that could handle an image including multiple cells [5] and demonstrated its application to high-speed focusing of yeast cells. However, these image processing algorithms were developed for specialized parallel vision systems [6], [7] with parallel processing elements. Conventional computers with single processors cannot run these algorithms.

In this paper, we propose a new serial image processing algorithm to achieve high-speed autofocusing of cells. The performance of the proposed algorithm was demonstrated by quick autofocusing of yeast cells. The effectiveness of the algorithm for high-speed measurement of cells was confirmed by demonstrating dynamic autofocusing of a field-scanning microscope that shifts its field of view automatically to measure a large number of cells.

II. DEPTH FROM DIFFRACTION METHOD

Depth estimation of target cells is essential for autofocusing. The "depth from diffraction" (DFDi) method estimates their depth from just one defocused image by using optical characteristics of cells.

Consider a cell observed with a microscope under Köhler illumination [8]. When the target cell is in focus, a clear image of the cell is observed. If we adjust the focus slightly

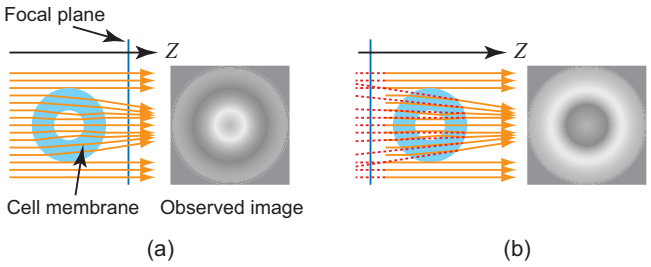

Fig. 2. Relationship between focal plane position and features of the acquired image. Two illustrations are shown to explain the diffraction pattern generation qualitatively: (a) the object is in front of the focal plane and a bright fringe appears inside the cell, or (b) the object is behind the focal plane and a bright fringe appears outside the cell.

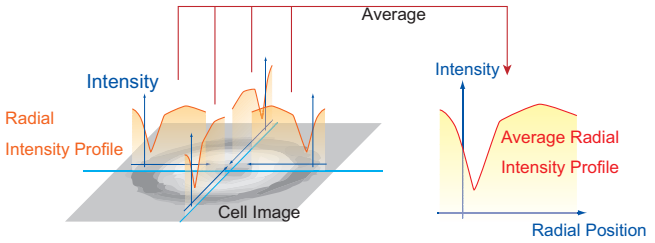

Fig. 3. Schematic diagram of the extraction process of the radial intensity profiles and their average. Four radial intensity profiles are extracted for each cell.

to defocus the image, bright and dark diffraction fringes can be observed near the periphery of the cell. For example, Fig. 1 shows these fringes in images of paramecium and yeast cells.

The mechanism of the diffraction pattern generation can be explained qualitatively by modeling the cell as a spherical shell. Fig. 2 shows a schematic diagram illustrating the diffraction pattern generation. It is assumed that the cell is illuminated by planar monochromatic light from the left, and the incident light is refracted mainly by the cell membrane. The membrane acts as a lens for the light rays that go through the membrane but not through the inside of the cell. The cell affects the rays in two ways. One set of rays passes through the side of the cell (and not the center). These are deflected inward. A second set of rays passes through one side of the cell, the cell's center, and then the other side. These are deflected by only a small amount. Thus, when the focal plane is behind the cell, we can observe a real image with a bright fringe inside and a dark fringe outside. Conversely, when the cell is behind the focal plane, we can observe a virtual image with a bright fringe outside and a dark fringe inside.

Although the above discussion is based on paraxial rays, Fresnel's diffraction theory [9] should be adopted for a more rigorous treatment of the phenomenon [4].

We concentrate on two useful characteristics of these fringes: first, the interval of the fringes depends on the distance between the focal plane and the target cell; and second, the order of the bright and dark fringes depends on the positional relationship between the focal plane and the cell. These characteristics suggest that the depth of the target cell could be estimated from a single defocused image of the cell containing such diffraction fringes. A similar phenomenon known as Becke lines is used in optical mineralogy [10], [11] to determine the refractive index of a transparent mineral.

Based on this idea, we previously proposed a new depth estimation method using the diffraction fringes of a cell [4]; we called this method "depth-from-diffraction", or DFDi. Since this method can estimate the depth from only a single defocused image, the depth estimation can be performed extremely rapidly. Once the depth is estimated, focusing can be easily realized by moving the focal plane to the estimated depth, or by moving the specimen to the focal plane.

Although we have confirmed the validity of the DFDi-method only for paramecium ($\phi \sim 100\mu$m) and yeast ($\phi \sim 5\mu$m) cells, we expect this method could be applied to many spherical and ellipsoidal cells, as well as transparent micro-beads.

Depth estimation methods of microscopic objects using two cameras have also been studied by other groups [16], [17]. In these methods, the optical path of a microscope is split into two to acquire two images from different viewpoints. However, splitting the optical path decreases the intensity of the image. Since microscope images tend to be quite dark to begin with, this may cause insufficient intensity for observation. In contrast, the DFDi method could be applied to a conventional microscope system with just one computer vision sensor and a conventional mechanical stage.

Furthermore, note that an origin in the depth direction can be defined on a physical basis using the DFDi method by setting the origin at the focal depth where no bright or dark fringes are observed. The focal plane should be located at the depth where the cell membrane is parallel to the optical axis, considering the mechanism of diffraction pattern generation of a spherical cell shown in Fig. 2. This means that a three-dimensional coordinate system of each cell can be defined based on its shape, since a two-dimensional origin (in X and Y directions) can be defined easily as the image centroid of the cell, for example.

III. SERIAL IMAGE PROCESSING ALGORITHM FOR DFDI

A serial image processing algorithm was developed to estimate a specimen's depth from its diffraction pattern. The algorithm was developed based on the assumption that each cell is spatially separated and not in contact with another cell. This assumption is satisfied when the specimen is an isolated floating cell, such as a blood or yeast cell. Even when the target cells are in the form of tissue, some of them can be dissociated into isolated cells using well-known techniques, for example, by using enzymes or surfactants. Thus, this assumption is realistic. In this study, yeast cells were adopted as the specimen.

Three photographs in the upper row of Fig. 1 are yeast images captured by a CCD camera mounted on the microscope. The following features of the diffraction pattern can be obtained from this figure.

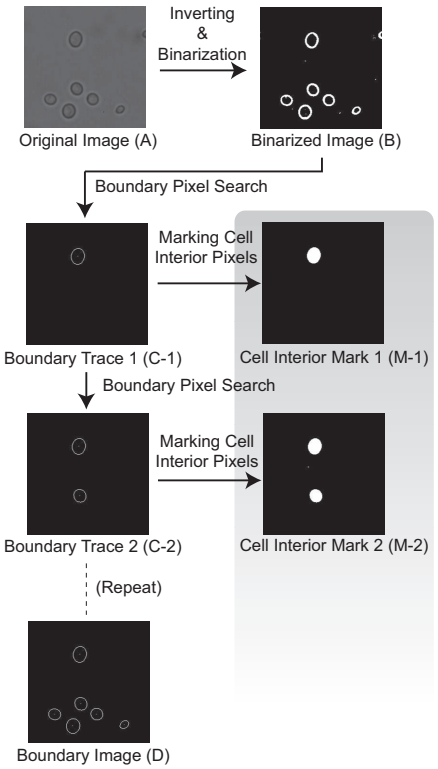

Fig. 4. Flow chart of the proposed image processing algorithm.

- When the specimen is farther from the objective lens than the focal plane, the interior of the cell becomes bright.
- When the specimen is nearer than the focal plane, a bright fringe appears outside the cell.

Consider a half-line originating at the center of the cell. The two features noted above indicate that the intensity profile near the cell boundary along this half-line varies with the profile shape, depending on the depth of the cell. Fig. 3 schematically illustrates the radial intensity profile, showing that the cell depth can be estimated from this profile. Thus, we concentrate on the radial intensity profile.

A. Cell boundary recognition

To extract the radial intensity profile, the algorithm needs to recognize a single cell and its boundary. Our algorithm extracts a single cell by extracting its boundary using a well-known boundary tracing algorithm and Freeman chain code [12], [13].

A captured microscope image A has a bright background and dark cell boundaries, as shown in Fig. 4 (A). By binarizing A with a suitable threshold, donut-shaped cell boundaries B are obtained, as shown in Fig. 4 (B).

A pixel on a cell boundary is found by searching for a pixel whose intensity was bright and whose left neighbor pixel was dark, by raster scanning. The found pixel is called the first boundary pixel a_1.

The cell boundary on which pixel a_1 is located is traced using a well-known boundary tracing algorithm. Let

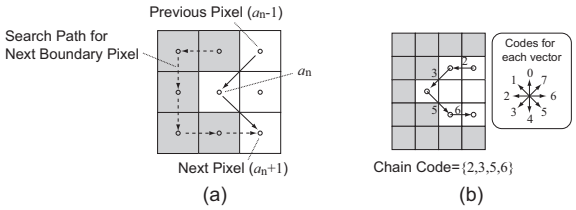

Fig. 5. Schematic illustration of (a) boundary pixel search, and (b) example of boundary tracing. Each square represents a pixel. White pixels are the object, and gray pixels are the background.

$a_1, a_2, \cdots a_n$ be boundary pixels. The next boundary pixel a_{n+1} is searched for from all 8 neighbouring pixels of a_n. The search path is in a clockwise direction and starts at the next pixel for the previous pixel a_{n-1}, as shown in Fig. 5 (a). When a boundary pixel is found, that pixel is recognized as the next pixel a_{n+1}. Then, treating a_{n+1} as the new current pixel, the algorithm proceeds in the same manner. This tracing stops when the next boundary pixel a_m satisfies $a_m = a_1$.

The boundary is represented by a Freeman chain code [12]. This chain code represents a boundary curve as a sequence of connections between one pixel and its neighbors. Eight vectors represent connections between one pixel and its 8-neighbours, respectively. These vectors are coded as 0, 1, $\cdots$ 7 so that the curve can be represented by the sequence of these numbers and the first boundary pixel, as shown in Fig. 5 (b).

Each yeast cell becomes a donut-shaped pattern in the binarized image B, as shown in Fig. 4 (B). This donut-shaped pattern has two boundary curves forming the outer and inner circular edges of the pattern. Although only the outer boundary of the pattern is of interest, the inner boundary might be detected by the boundary tracing process. To prevent such incorrect detection, all of the pixels inside the detected boundaries are marked as *cell interior* whenever the boundary tracing ends so that only the outer boundaries of cells are recognized. This also prevents redetection of another pixel on the already detected cell boundary. Fig. 4 (M-1) and (M-2) show the images of *cell interior* marks.

After marking the cell interiors, another pixel without the *cell interior* mark is searched for by raster scanning. If another boundary pixel is found, the same boundary tracing process is performed in the same manner. The boundary searching and tracing are repeated until the raster scanning reaches the bottom-right pixel.

B. Extraction of the radial intensity profile

The radial intensity profiles of each cell are extracted after the boundary recognition.

Each radial intensity profile is represented as a set of intensity values of thirteen pixels. These pixels are selected in order of their distance from the cell boundary, namely, -8, -6, -4, 2, 0, 2, 4, 6, 8, 10, 12, 14, and 16. A negative distance means that the pixel is outside the cell. The distances are calculated from the cell center position and a given position

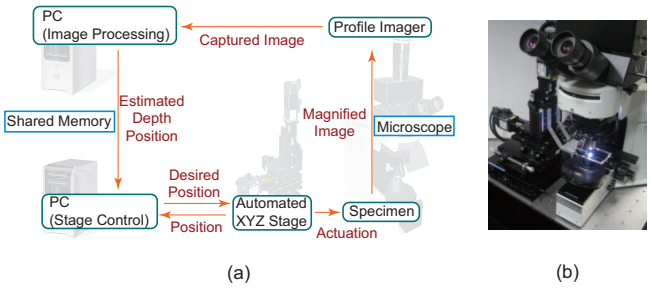

Fig. 6. Block diagram of the experimental set-up (a), and a photograph of the microscope with the XYZ stage (b). A slide glass including specimens was fixed on the XYZ stage using a metal frame.

on the cell boundary. The center position of each cell is calculated as the image centroid of its boundary pixels.

For each cell, four profiles are extracted so that an average profile can be obtained to reduce noise included in the intensity values, as shown in Fig. 3.

C. Depth estimation by linear regression

The depth of a cell is estimated by multiple linear regression of its average radial intensity profile. We assume that the relationship between a cell's depth and its average radial intensity profile is linear and capable of being represented by the following equation:

$$Z = c_0 + c_1 i_1 + c_2 i_2 + \cdots + c_{13} i_{13}, \qquad (1)$$

where Z is the depth of the target cell, $i_1, i_2, \cdots i_{13}$ are the average radial intensity profiles, and $c_0, c_1, \cdots c_{13}$ are coefficients of the linear regression. These coefficients are calibrated using cell images captured at various depths.

IV. EXPERIMENTS

A. Experimental set-up

To verify the effectiveness of the proposed algorithm experimentally, we developed the experimental set-up shown in Fig. 6. The set-up consisted of an optical microscope (BX50WI, Olympus), a computer vision system (Profile Imager), an XYZ automated stage, a personal computer (PC) for stage control, and another PC for image processing. Both PCs were connected via a shared memory, allowing them to communicate with each other.

A bright-field image of target cells with Köhler illumination was magnified with a 100-times objective lens (NA 0.95, UMPlanFl, Olympus) and projected onto the vision system.

To realize high-speed focusing, the vision system must be capable of high-speed image acquisition and processing. Therefore, the vision system we adopted was the so-called Profile Imager system developed by Hamamatsu Photonics K. K. [14], a high-speed CMOS imager with adaptive readout of a region-of-interest (ROI). In our experiment, the ROI was set to 232×232 pixels at 1-kHz frame rate. The effective view field of the Profile Imager was 46.4 × 46.4 μm.

The image processing PC included two dual-core Intel Xeon 3.0-GHz processors running Microsoft Windows XP. An image processing program was developed using the C++ language with an Intel C++ compiler and Microsoft Visual Studio. The PC could execute all image processing algorithms, including binarization, boundary detection, extraction of radial intensity profiles, and depth estimation, within 1 ms when the 232×232 grayscale image included one yeast cell.

The estimated depth information was transmitted to the other stage control PC having an Intel Pentium4 3.2-GHz processor running a real-time OS (ART-Linux, Moving Eye). This PC controlled the position of the XYZ stage to the desired position. The control period was 1 ms.

A slide including the yeast cells was fixed on the XYZ stage so that its position could be controlled in three dimensions. The stage's specifications are shown in Table IV-A. The step response time of all axes was around 50 ms. All axes were actuated by AC servomotors (HF-KP053(B), Mitsubishi Electric) driven by AC servo amplifiers (MR-J3-10A, Mitsubishi Electric).

TABLE I
SPECIFICATIONS OF THE XYZ AUTOMATED STAGE

Specifications	X axis	Y axis	Z axis
Stroke	25 mm	25 mm	10 mm
Sensor resolution	0.25 μm	0.25 μm	0.25 μm
Repeatability	$\pm$1 μm	$\pm$1 μm	$\pm$1 μm

B. Depth estimation using radial intensity profiles

The average radial intensity profiles of a yeast cell were measured at various depths to confirm that the profiles actually depended on the depth of the cell. This experiment required high positional resolution in the depth direction. Thus, we used a piezoelectric stage (P-731.10, PI GmbH & Co. KG.) that had a high positional resolution of <1.0 nm instead of the XYZ stage. The piezoelectric stage was used for the experiments described in IV-B and IV-C.

A yeast cell was held on a slide glass with its medium covered by a cover glass. The cell was placed at the center of the field of view of the microscope. The radial intensity profiles were measured by scanning the depth of the cell from -6 μm to +6 μm in 0.1 μm steps. The depth origin was defined as the depth when an observer recognized that the cell was in focus. Positive depth means that the cell was nearer the objective lens than the focal plane of the microscope.

Fig. 7 shows three of the measured profiles at -4, 0, and +4 μm in depth. The following characteristics were obtained from this figure.

- When the cell was in focus, the intensities of pixels outside the cell and those of pixels inside the cell were almost identical.
- When the cell depth was +4 μm, the outside of the cell was brighter than the inside.
- When the cell depth was -4 μm, the inside of the cell was brighter than the outside.

The results confirmed that the profile depended on the depth of the cell.

The linear regression coefficients were estimated from the measured radial intensity profiles using the least squares

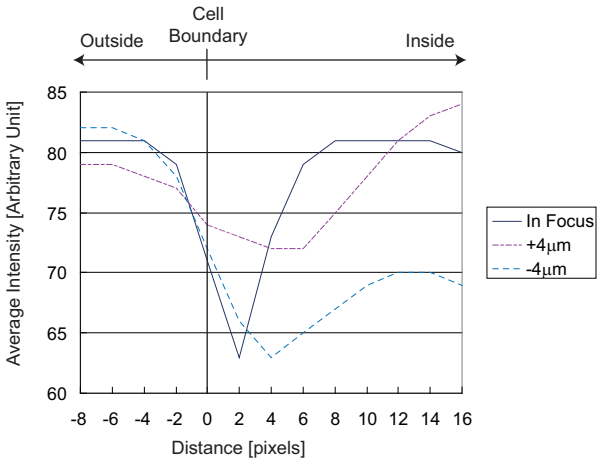

Fig. 7. Average radial intensity profiles measured at -4, 0, and +4 μm in depth.

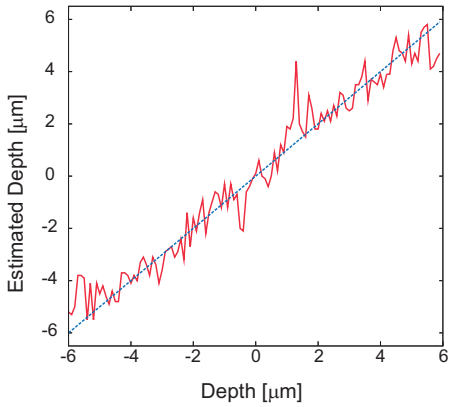

Fig. 8. Estimated depth of the yeast cell versus its actual depth.

method. Fig. 8 shows the estimated depth profile versus the actual depth of the target cell. The maximum residual was about 1 μm, almost the same as the typical depth of focus of the microscope. Thus, the assumed model was sufficiently valid for microscope autofocusing.

C. High-speed autofocusing

An autofocusing experiment involving yeast cells was conducted to confirm the high-speed focusing ability of the proposed algorithm.

In this experiment, the image processing PC captured an image of the cells and estimated their depth. The estimated depth was transmitted to the control PC, which then controlled the Z position of the specimens so that they were in focus.

To evaluate the autofocusing speed, a step response of the depth was measured. First, average radial intensity profiles of yeast cells at various depths were measured to calibrate the linear regression coefficients. Next, the cells were defocused by -5 μm initially. Then, autofocus control was started at time $t = 0$.

The focusing speed was evaluated as a settling time of the response. Fig.9 shows the step response of the depth of the

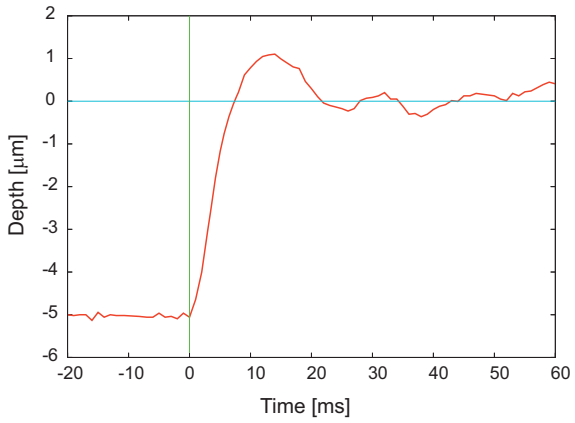

Fig. 9. Step response of the cell depth.

target. The settling time was about 20 ms, though the depth estimation took only 1 ms. The residual response time was due to the step response time of the piezo stage. The settling time was much shorter than the typical response time of 0.8 s of conventional autofocus systems.

D. Continuous autofocusing for a scanning microscope

The developed autofocusing algorithm was applied to a scanning microscope to show its effectiveness in a realistic application. When the number of specimens is large, it is impossible to observe all specimens in a static field of view of a microscope due to the limited resolution of the microscope or camera. A scanning microscope solves this problem by moving its field of view to observe the specimen as a sequence of images. Scanning microscopes are commonly used in the field of cytometry [15].

Autofocusing is essential for the scanning microscope to obtain a precise image of the specimen. It is not possible to maintain focus simply by determining the best focus depth at two points on a microscope slide and scanning along the line between them in three-dimensional space [1]. There may be many reasons for this, including mechanical instability of the microscope and irregularity of the glass slide surface.

The purpose of this experiment was to keep the cells in focus while scanning the field. A slide glass holding many yeast cells was fixed on the XYZ-stage described in IV-A.

When one or more cell(s) was included in the image captured by the profile sensor, the depth of a cell located at the upper-leftmost position in the image was estimated. The Z axis of the stage was controlled to bring the estimated cell into focus according to the estimated depth. When no cell was in the image, the Z-axis was controlled to keep the previous position. The X- and Y-axes were controlled to scan a given rectangular outline at a constant velocity of 250 μm/s. This velocity corresponded to 5.4 widths of the field per second in our experimental set-up. The linear regression coefficients were previously estimated for a typical yeast cell with the same illumination conditions adopted in this experiment.

Fig. 10 shows the images captured while focusing cells entering the field of view. When two cells entered the field

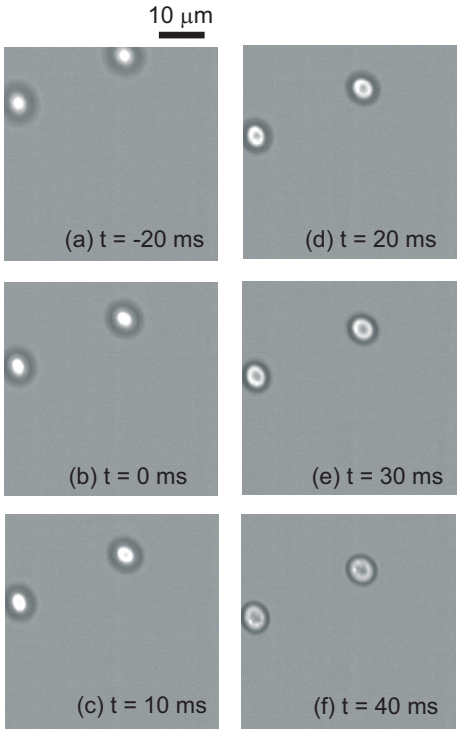

Fig. 10. Images captured by the profile imager while focusing cells entering the field of view.

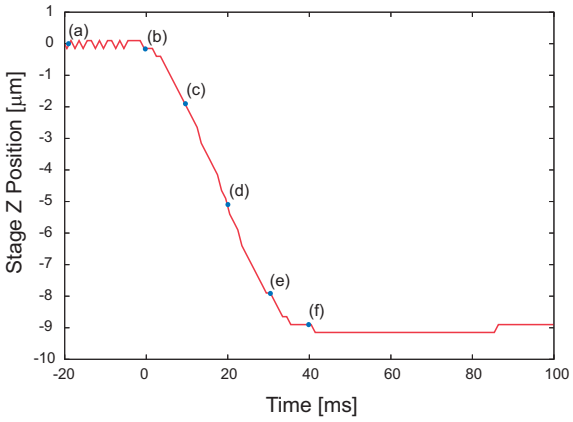

Fig. 11. Trajectory of the Z-axis position. Points denoted by letters correspond to the images shown in Fig. 10

of view shown in Fig. 10 (a), they were not focused. The autofocusing was started when the right cell had entered the field completely in (b). Upon completion of autofocusing, the two cells were in focus (f). Fig. 11 shows the trajectory of the Z-axis during this focusing. The stage was kept at its depth position after the cells were in focus ($t > 40$ms). A video of this experiment is also available [18].

By using our autofocusing algorithm, a scanning microscope could scan the field at high speed while keeping the specimen in focus. This suggested that image-based high-throughput measurement or screening of cells could be realized using a scanning microscope.

Current high-throughput cytometers, such as flow cytometers, cannot recognize spatial information, such as the protein distribution in a cell. This drawback could be overcome by using the proposed algorithm.

V. Conclusion

In this paper, a new serial algorithm for high-speed autofocusing of cells was proposed. The proposed algorithm extracts depth information of target cells from their diffraction patterns based on the depth-from-diffraction (DFDi) method. High-speed focusing of yeast cells with 20-ms response time was demonstrated. The algorithm was also applied to the continuous autofocusing of a scanning microscope. The successful continuous autofocusing suggests that image-based high-throughput measurement of cells could be realized using the proposed algorithm.

References

[1] J. H. Price and D. A. Gough, "Comparison of Phase-Contrast and Fluorescence Digital Autofocus for Scanning Microscopy," *Cytometry*, vol. 16, no. 4, pp. 283–297, 1994.

[2] M. Subbarao and J.-K. Tyan, "Selecting the Optimal Focus Measure for Autofocusing and Depth-From-Focus," *IEEE Trans. Pattern Anal. Machine Intell.*, vol. 20, no. 8, pp. 864–870, 1998.

[3] J.-M. Geusebroek, F. Cornelissen, A. W. M. Smeulders, and H. Greets, "Robust Autofocusing in Microscopy," *Cytometry*, vol. 39, no. 1, pp. 1–9, 2000.

[4] H. Oku, M. Ishikawa, Theodorus, and K. Hashimoto, "High-speed autofocusing of a cell using diffraction pattern," *Optics Express*, vol. 14, no. 9, pp. 3952–3960, 2006.

[5] S. Makise, H. Oku, and M. Ishikawa, "High-speed autofocus on cell group using diffraction pattern (in Japanese)," *Proc. JSME Conf. on Robotics and Mechatronics (Robomec 2006)*, pp. 1A1–C28, 2006.

[6] M. Ishikawa, K. Ogawa, T. Komuro, and I. Ishii, "A CMOS Vision Chip with SIMD Processing Element Array for 1ms Image Processing," *Digest of Technical Papers of IEEE Int. Solid-State Circuits Conf. (ISSCC)*, pp. 206–207, 1999.

[7] H. Toyoda, N. Mukohzaka, K. Nakamura, M. Takumi, S. Mizuno, and M. Ishikawa, "1ms column-parallel vision system coupled with an image intensifier; I-CPV (in Japanese)," *Proc. of Symp. High Speed Photography and Photonics 2001*, vol. 5-1, pp. 89–92, 2001.

[8] M. Born and E. Wolf, *Principles of Optics, 7th Edition*. Cambridge University Press, 2002.

[9] J. W. Goodman, *Introduction to Fourier Optics*. McGraw-Hill, Inc., 1996.

[10] W. D. Nesse, *Introduction to Optical Mineralogy*. Oxford University Press, New York, 1991.

[11] T. Tsuruta, *Oyo-kogaku(applied optics) I (in Japanese)*. Baifukan, 1990.

[12] H. Freeman and A. Saghri, "Generalized chain codes for planar curves," *Proc. of the 4th Int. Joint Conf. on Pattern Recognition*, pp. 701–703, 1978.

[13] A. Rosenfeld and A. C. Kak, *Digital Picture Processing*. Academic Press, New York, 1976.

[14] Y. Sugiyama, M. Takumi, H. Toyoda, N. Mukozaka, A. Ihori, T. Kurashina, Y. Nakamura, T. Tonbe, and S. Mizuno, "A High-Speed, Profile Data Acquiring Image Sensor," *Digest of Technical Papers of IEEE Int. Solid-State Circuits Conf. (ISSCC)*, vol. 1, pp. 360–361, 2005.

[15] H. M. Shapiro, "Cellular Astronomy - A Foreseeable Future in Cytometry," *Cytometry Part A*, vol. 60A, no. 2, pp. 115–124, 2004.

[16] P. F. M. Teunis, F. Bretschneider, and H. Machemer, "Real-time three-dimensional tracking of fast-moving microscopic objects," *J. Microscopy*, vol. 168, pp. 275–288, 1992.

[17] M. Shimazu, T. Tsuji, K. Yamamoto, and I. Ishii, "Three Dimension Tracking System on Microscopic Using Two High-speed Mega Pixel Visions (in Japanese)," *Proc. JSME Conf. on Robotics and Mechatronics (Robomec 2006)*, pp. 2A1–C11, 2006.

[18] `http://www.k2.t.u-tokyo.ac.jp/mvf/index-e.html`